Research Article

Fluorescence and Nonradiative Properties of Nd³⁺ in Novel Heavy Metal Contained Fluorophosphate Glass

Ju H. Choi,[1] Alfred Margaryan,[2] Ashot Margaryan,[2] Frank G. Shi,[1] and Wytze Van Der Veer[3]

[1] *Department of Chemical Engineering and Materials Science, University of California, Irivne, CA 92697, USA*

[2] *AFO Research Inc., P.O. Box 1934, Glendale, CA 91209, USA*

[3] *Department of Chemistry, University of California, Irvine, CA 92697, USA*

We demonstrate new series of heavy metal containing fluorophosphate glass system. The fluorescence and nonradiative properties of Nd³⁺ ions are investigated as a function of Nd_2O_3 concentration. The variation of intensity parameters Ω_2, Ω_4, and Ω_6 is determined from absorption spectra. The spontaneous probability (A) and branching ratio (β) are determined using intensity parameters. The emission cross sections for the $^4F_{3/2} \rightarrow {}^4I_{13/2}$ transition, which is calculated by Fuchtbabauer-Ladenburg method, decrease from 6.1×10^{-21} to 3.0×10^{-21} (pm²) and those for the $^4F_{3/2} \rightarrow {}^4I_{11/2}$ transition decrease from 3.51×10^{-20} to 1.7×10^{-20} as Nd_2O_3 concentration increase up to 3 wt%. The nonradiative relaxation is analyzed in terms of multiphonon relaxation and concentration quenching due to energy transfer among Nd³⁺ ions. Finally, the above results obtained at 1 wt% Nd_2O_3 are compared with some of reported laser host glasses which indicated the potentials for broadband-amplifiers and high-power laser applications.

1. INTRODUCTION

Over the past several decades, optical and spectroscopic properties of various trivalent lanthanides have been extensively investigated for various host materials to apply optical devices. Among many trivalent lanthanides, researches on Nd³⁺-doped glasses have been performed because Nd³⁺-doped fiber has attracted much interest for optical amplifier at the region around 1325 nm with the rapid development of telecommunications as well as around 1050 nm for high-power laser applications [1–3]. In general, the optical and spectroscopic properties are strongly dependent on host materials. Many potential host materials for rare earth ions have been developed. Among them, fluorophosphates glasses show outstanding advantages such as low phonon energy, transmittance from UV to IR spectral range, and low nonlinear refractive index [4–6]. It was also found that with a fluorophosphate glass, a relatively higher degree of line broadening and smoother line shapes can be obtained [7]. It was also observed that Nd³⁺-doped fluorophosphate glasses can deliver relatively shorter pulses than pure phosphate glasses, which were attributed to the relatively higher degree of inhomogeneous line broadening in fluorophosphate glasses [8].

Those advantages can represent one of the best potential host materials for several rare earth dopants for laser applications [9–11]. Typically, heavy metal contained glasses have been used for nonlinear photonic devices such as switchinhg. The efforts to improve quantum efficiency of the luminescence bands have paid attention to heavy metal contained host materials as well as active ion concentration. The host glass materials should also have high refractive index with good chemical and thermal stability along with low melting temperature of heavy metals in order to become more practical usage in industry. Spectroscopic and optical properties based on fluorophosphates glass doped with Yb³⁺ and Nd³⁺ were successfully investigated and presented strong potentials as gain medium in our previous works [12–15].

The purpose of this paper is to introduce the upgraded fluorophosphates glasses by including the heavy metal contained phosphate compositions. The newly developed $Bi(PO_3)_3 - Ba(PO_3)_2 - BaF_2 - MgF_2$ glass system (BBBM system) with different amounts of Nd_2O_3 have been systematically investigated on spectroscopic properties. Intensity parameters, emission cross section, radiative lifetime, branching ration, and fluorescence quantum efficiency are

determined from the absorption and the emission spectra using Judd-Ofelt parameter theory. The trend of spectroscopic properties between the $^4F_{3/2} \rightarrow {}^4I_{13/2}$ and the $^4F_{3/2} \rightarrow {}^4I_{11/2}$ are investigated as a function of Nd_2O_3.

2. EXPERIMENTS AND DATA ANALYSIS

2.1. Glass synthesis and measurements

Starting materials from reagent grade (city chemicals) and Nd_2O_3 (spectrum materials) have above 99.99% purity. A series of glasses were weighed on 0.001% accuracy according to mole ratio $(20Bi(PO_3)_3 - 10Ba(PO_3)_2 - 35BaF_2 - 35MgF_2)$ and mixed thoroughly. The raw mixed materials were melted in a vitreous carbon crucible in Ar-atmosphere at 1200–1250°C. The quenched samples were annealed at transition temperature below 50–100°C to remove an internal stress. The residual stress was examined by the polariscope (rudolph instruments). Samples for optical and spectroscopic measurements were cut and polished by the size of $15 \times 10 \times 2\,mm^3$. The refractive index of the samples was measured using an Abbe refractometer (ATAGO). The absorption spectra were recorded at room temperature in the range of 400–1700 nm with a Perkin-Elmer photo spectrometer (Lambda 900). The resolution is set to 1 nm. Emission spectra are obtained by exciting the samples with 808 nm radiation from a CW laser diode (coherent). The fluorescence radiation is then recorded over the range 850–1400 nm using a monochromator (Acton SpectraPro 300) and a ge-photodiode (Thorlabs). The laser radiation incident to the sample is passed through an optical chopper (Stanford Research) enabling the use of a lock-in amplifier (Ametek 5105) to recover and amplify the electronic signal from the detector. The lifetime of the excited state is determined with a Q-switched Nd:YAG laser pumping an OPO (continuum surelite) tuned to 808 nm (idler). The duration of the pulses is 5 nanoseconds. The fluorescent radiation is detected using a Si pin photodiode (Thorlabs) and an interference filter (Edmund Scientific). The signal is recorded with a fast oscilloscope (LeCroy 9350) and fitted to an exponential.

2.2. Judd-Ofelt theory

Judd-Ofelt theory has been used to investigate radiative nature of trivalent rare earth ions in a variety of laser host materials [16, 17]. The absorption spectra of rare earth ions of $4f$-$4f$ electronic transitions are from electric dipole, magnetic dipole, and electric quadrupole. The intensity parameter, radiative lifetime, and branching ratio are calculated with refractive index using Judd-Ofelt analysis. The theoretical oscillator strengths f_{cal} are derived by using the Judd-Ofelt theory. Theoretical oscillator strengths $f(aJ, bJ')$ of the $J \rightarrow J'$ transition at the mean frequency ν are given for an electric and magnetic dipole transition by

$$f_{cal}(aJ, bJ') = \frac{8\pi^2 m\nu}{3(2J+1)he^2n^2}[\chi_{ED}S_{ED}(aJ, bJ')], \quad (1)$$

where m is the mass of the electron, e and h are the charge of the electron and Plank's constant, respectively. $\chi_{ED} =$

TABLE 1: Values of reduced matrix elements for the chosen emission of Nd^{3+} in $Bi(PO_3)_3 - Ba(PO_3)_2 - BaF_2 - MgF_2$ glass systems.

Transition from $^4F_{3/2}$	λ (nm)	$[U^{(2)}]^2$	$[U^{(4)}]^2$	$[U^{(6)}]^2$
$^4I_{15/2}$	1824	0	0	0.0280
$^4I_{13/2}$	1324	0	0	0.2120
$^4I_{11/2}$	1054	0	0.142	0.4070
$^4I_{9/2}$	899	0	0.23	0.056

$n(n^2 + 2)^2/9$ and $\chi_{MD} = n^3$ are local field corrections and are functions of the medium refractive index n. S_{ED} is the electrical dipole line strength, respectively, and is given by

$$S_{ED}(aJ, bJ') = e^2 \sum_{t=2,4,6} \Omega_t |\langle 4f^N aJ || U^{(t)} || 4f^N bJ' \rangle|^2, \quad (2)$$

where the reduced matrix elements of the unit tensor operators, $\langle || \mathbf{U}^{(t)} || \rangle$, are calculated in the intermediate-coupling approximation. They are found to be almost invariant to the environment and are given by Carnall et al. [18]. The values of reduced matrix elements and the mean wavelength of the chosen emission bands of Nd^{3+} were tabulated in Table 1. The measured oscillator strengths f_{med} at each absorption wavelength can be calculated from the integrated optical absorption spectra and are given by following expression from

$$f_{med} = \frac{mc^2}{\pi e^2 N} \int \frac{\alpha(\lambda)}{\lambda^2} d\lambda, \quad (3)$$

where c is light velocity, N is the Nd^{3+} ion concentration (ion/cm³). $\alpha(\lambda)$ (= $2.303D_0(\lambda)/d$) is the measured optical absorption coefficient at a particular absorption wavelength λ and d is the sample thickness.

The oscillator strengths both experimentally and theoretically obtained are presented in Table 2. In order to evaluate the validity of the intensity parameters, the deviation parameter was obtained by the root-mean-square (rms, δ_{rms})

$$\delta_{rms} = \left[\frac{\sum(f_{cal} - f_{med})^2}{N_{par} - N_{trans}} \right], \quad (4)$$

where N_{par} is the number of spectral bands analyzed and N_{trans} are 3 in this case, which is the parameter number sought. The values of δ_{rms} within 5×10^{-6} imply the good fitting between the measured f_{med} and the theoretical f_{cal} oscillator strengths. These Judd-Ofelt parameters obtained from the fitting between the measured f_{med} and the theoretical f_{cal} oscillator strengths can be also applied to calculate the line strength corresponding to the transitions from the initial J manifold and the final J' manifold.

The radiative transition probabilities given in (5) were obtained with the line strength for the excited $^4F_{3/2}$ to $^4I_{J'}$ manifold ($^4I_{9/2}$, $^4I_{11/2}$, and $^4I_{13/2}$) for Nd^{3+}:

$$A_{rad}[aJ, bJ'] = \frac{64\pi^4}{3h(2J+1)\lambda^3}\left[\frac{n(n^2+2)^2}{9}S_{ED}(aJ, bJ')\right], \quad (5)$$

TABLE 2: Experimental and calculated oscillator strengths ($f \times 10^6$) of Nd^{3+} in $20Bi(PO_3)_3 - 10Ba(PO_3)_2 - 35BaF_2 - 35MgF_2$ glass system at room temperature.

Transition from $^4I_{9/2}$	Energy (cm^{-1})	0.5 wt%		1 wt%		1.5 wt%		3 wt%	
		f_{med}	f_{cal}	f_{med}	f_{cal}	f_{med}	f_{cal}	f_{med}	f_{cal}
$^4F_{3/2}$	11442	1.71	3.45	2.52	3.24	2.20	3.21	1.17	1.58
$^4F_{5/2}$	12469	8.10	9.27	8.55	8.64	8.24	8.75	4.33	4.46
$^4F_{7/2}$	13405	9.05	8.80	8.05	8.17	8.46	8.38	4.35	4.35
$^4F_{9/2}$	14684	1.13	0.72	0.53	0.67	0.55	0.68	0.20	0.35
$^4G_{5/2}$	17182	19.12	19.20	16.48	16.53	17.20	17.25	8.83	8.84
$^4G_{7/2}$	19048	8.81	7.37	7.16	6.79	7.88	6.85	3.78	3.44
$^2K_{15/2}$	21008	5.33	1.75	3.19	1.64	3.08	1.64	1.48	0.82
$^1P_{1/2}$	23310	0.53	0.96	0.35	0.90	0.21	0.89	0.15	0.43

TABLE 3: Theoretically calculated radiation transition probability, branching ratios radiative lifetime, and quantum efficiency of Nd^{3+} in $20Bi(PO_3)_3 - 10Ba(PO_3)_2 - 35BaF_2 - 35MgF_2$ glass system at room temperature.

Transitions from $^4F_{3/2}$	Energy (cm^{-1})	0.5 wt%		1.0 wt%		1.5 wt%		3 wt%	
		A (s^{-1})	β (%)	A (s^{-1})	β (%)	A (s^{-1})	β (%)	A (s^{-1})	β (%)
$^4I_{13/2}$	7508	358	8.5	333	8.4	343	8.6	179	8.9
$^4I_{11/2}$	9443	1948	46.1	1817	45.9	1849	46.4	946	47.1
$^4I_{9/2}$	11186	1922	45.5	1808	45.7	1796	45.0	884	44.0
$A_T = \sum A$ (s^{-1})		4229		3958		3989		2009	
τ_{rad} (μs)		237		253		251		498	
Quantum efficiency		76%		67%		62%		30%	

where $n(n^2+2)^2/9$ is the local field correction for Nd^{3+} in the initial J manifold. J' is the final manifold. n is the refractive index at the wavelength of the transition.

The emission branching ratio for transitions originating from initial manifold can be obtained from the radiative transition probabilities A_{rad} by using

$$\beta(^4F_{3/2} \longrightarrow {}^4I_J) = \frac{A(^4F_{3/2} \longrightarrow {}^4I_J)}{\sum_J A(^4F_{3/2} \longrightarrow {}^4I_J)}, \qquad (6)$$

where the summation is over all terminal manifolds. Theoretically computed radiative properties of Nd^{3+} in the current system including radiative transition probabilities, branching ratio ratios radiative lifetime and quantum efficiency are listed in Table 3.

2.3. Stimulated emission cross-section

Laser transitions are also characterized by stimulated emission cross sections while the induced emission cross sections are characterized by Judd-Ofelt theory. The stimulated emission cross-section between $^4I_J \rightarrow {}^4I_{J'}$ is given by Fuchtbabauer-Ladenburg method [19]:

$$\sigma_{em} = \frac{\lambda_p^4}{8\pi c n(\lambda_p)^2 \Delta\lambda_{eff}} A(aJ, bJ'), \qquad (7)$$

where λ_p is the wavelength of the peak emission, c is the speed of light in vacuums, and $n(\lambda_p)$ is the refractive index at each emission peak wavelength. $\Delta\lambda_{eff}$ is an effective linewidth. Since the emission band is asymmetry, it is used instead of the full width at half maximum linewidth. It is characterized in the name of an effective linewidth as follows:

$$\Delta\lambda_{eff} = \frac{\int I(\lambda)d\lambda}{I_{max}}. \qquad (8)$$

I_{max} is the maximum intensity at fluorescence emission peaks.

3. RESULTS AND DISCUSSION

3.1. Absorption spectra analysis

The absorption spectra BBBM system doped with 3 wt% Nd_2O_3 recorded in the 400–950 nm at room temperature are shown in Figure 1. The absorption spectra of Nd^{3+} ions in BBBM system are corresponding to transitions from the ground state $^4I_{9/2}$ to various excited states within the $4f$ shell. The appropriate electronic transitions were assigned to these bands. The integrated area of the absorption band of the $^4I_{9/2} \rightarrow ({}^4F_{5/2} + {}^2H_{9/2})$ transition linearly increased and the refractive indices (n_D) increase from 1.6263 to 1.6355 in BBBM system as Nd_2O_3 concentration increases up to 3 wt%.
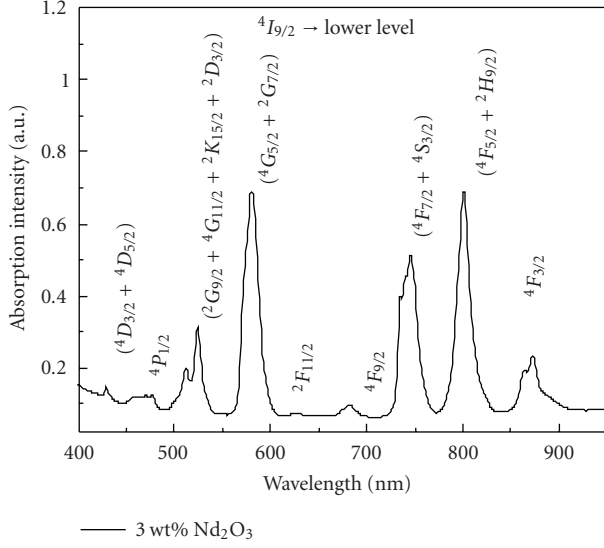
FIGURE 1: Absorption spectra of 3 wt% Nd^{3+} doped $Bi(PO_3)_3 - Ba(PO_3)_2 - BaF_2 - MgF_2$ glass system at room temperature.
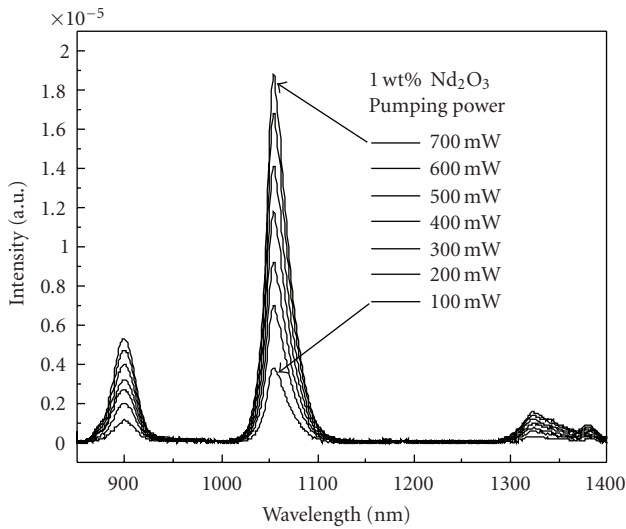
FIGURE 2: Emission spectra of 1.0 wt% Nd_2O_3 doped $Bi(PO_3)_3 - Ba(PO_3)_2 - BaF_2 - MgF_2$ glass system as a function of pumping power.

3.2. Fluorescence spectra analysis

Figure 2 shows the measured emission spectra of 1.0 wt% Nd_2O_3 doped BBBM system. Using the excitation wavelength of 808 nm, emission spectra were recorded at room temperature in the range of 750 nm to 1600 nm. Three emission spectra, which are centered at 876, 1058, and 1334 nm, present broad bands, which is well known that it is characteristic because of the inhomogeneous disordered glasses. The fluorescence intensities also increase as the pumping power increases. Figure 3 shows the fluorescence decay lifetime of Nd^{3+} for the $^4F_{3/2} \rightarrow {}^4I_{11/2}$ transition as a function of Nd_2O_3
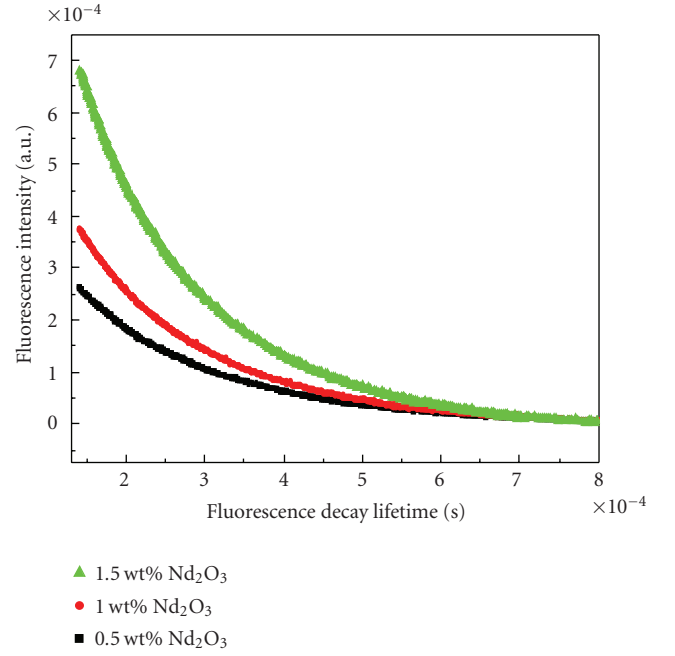

FIGURE 3: Fluorescence decay curves of Nd^{3+} for the $^4F_{3/2} \rightarrow {}^4I_{11/2}$ transition at room temperature as a function of concentration in the $Bi(PO_3)_3 - Ba(PO_3)_2 - BaF_2 - MgF_2$ glass system.

concentration. There is a linear decrease from 180 to 157 μs in fluorescence decay rate by measuring lifetime of the $^4F_{3/2}$ level as Nd_2O_3 concentration increases up to 1.5 wt%.

4. DISCUSSION

4.1. Dependence of intensity parameters on Nd_2O_3 concentration

The best set of Ω_t parameters was determined by a standard least-square fitting of the theoretical oscillator strength values to the measured ones. The variation of Judd-Ofelt parameters Ω_t for Nd^{3+} ions in the BBBM system is shown as a function of Nd_2O_3 in Figure 4. The intensity parameter Ω_2 for Nd^{3+} slightly decreases from 2.54×10^{-20} to 1.12×10^{-20} (pm^2) with increase in Nd_2O_3 concentration. The intensity parameters Ω_4, and Ω_6 for Nd^{3+} are also found to decrease from 6.86×10^{-20} to 3.09×10^{-20} and 5.74×10^{-20} to 2.87×10^{-20} (pm^2), respectively, with increase in Nd_2O_3 concentration from 0.5 wt% to 3 wt%. For $Bi(PO_3)_3 - Ba(PO_3)_2 - BaF_2 - MgF_2$ systems, the trend for the Ω_t parameters is $\Omega_2 < \Omega_6 < \Omega_4$. The tendency of intensity parameters is in agreement with those reported by Kumar et al. [20] and comparable with those of other fluorophosphates glasses [21, 22].

It is well known that the parameter Ω_2 exhibits the dependence on the covalency between rare earth ions and ligands anions, since Ω_2 reflects the asymmetry of the local environment at the Nd^{3+} ion site [23]. The relatively small value of Ω_2 (below 2.0×10^{-20} pm^2) exhibits the covalence in bonding [24]. In addition, the slight decrease of Ω_2 with an increase in Nd_2O_3 concentration indicates the decrease of
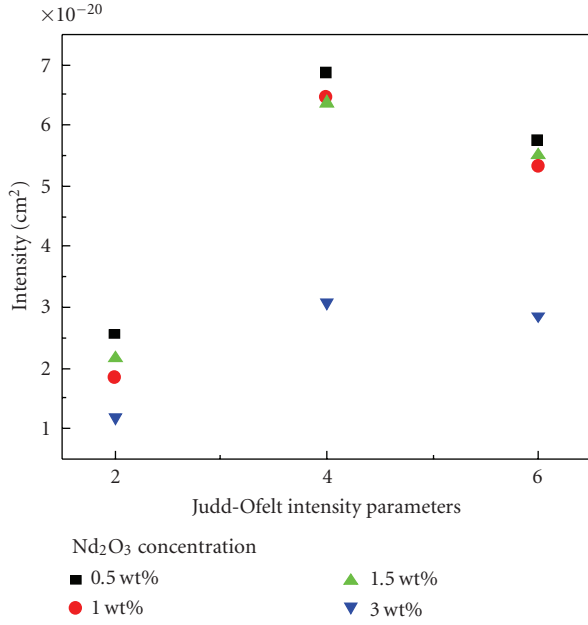
FIGURE 4: Variation of Judd-Ofelt parameters, Ω_t, for Nd^{3+} ions as a function of Nd_2O_3 in the $Bi(PO_3)_3-Ba(PO_3)_2-BaF_2-MgF_2$ glass system.

FIGURE 5: Dependence of the spectroscopic quality factor (η) as a function of Nd_2O_3 concentration in the $Bi(PO_3)_3-Ba(PO_3)_2-BaF_2-MgF_2$ glass system.

FIGURE 6: Variation of branching ratio (β) as a function of Nd_2O_3 concentration in the $Bi(PO_3)_3-Ba(PO_3)_2-BaF_2-MgF_2$ glass system.

covalency. Emission intensity could be also uniquely characterized by the Ω_4 and Ω_6 parameters because Ω_2 is not included to calculate branching ration for the laser $^4F_{3/2} \rightarrow {}^4I_{11/2}$ transition. It is called spectroscopic quality factor χ ($= \Omega_4/\Omega_6$) suggested by Jacobs and Weber [25].

4.2. Dependence of spectroscopic quality factor and branching ratio on Nd_2O_3 concentration

Figure 5 shows the dependence of the spectroscopic quality factor χ as a function of Nd_2O_3 concentration. χ is found to increase from 1.19 to 1.21 at 1 wt% Nd_2O_3 and then decrease 1.07 with increase in Nd_2O_3 concentration. Usually, χ is in the range from 0.22 to 1.5 for Nd^{3+} in several host materials [21]. For the relationship between the variation of χ and the $^4F_{3/2} \rightarrow {}^4I_{11/2}$ and $^4F_{3/2} \rightarrow {}^4I_{9/2}$ transition, it is reported that in the case of $\Omega_4 \geq \Omega_6$, the efficiency of the $^4F_{3/2} \rightarrow {}^4I_{11/2}$ transition is reduced and on the other hand the efficiency of the $^4F_{3/2} \rightarrow {}^4I_{9/2}$ transition is enhanced, for example, on the other hand, the smaller the value of χ, the more intense the laser $^4F_{3/2} \rightarrow {}^4I_{11/2}$ transition [26, 27]. Figure 6 shows the variation of branching ratio (β) with as a function of Nd_2O_3 concentration. It is observed that the values of β for the $^4F_{3/2} \rightarrow {}^4I_{9/2}$ transition slightly increase from 0.45 to 0.46 at 1 wt% and then decrease 0.44 at 3 wt%. Those of branching ratio for the $^4F_{3/2} \rightarrow {}^4I_{11/2}$ transition will show the opposite trends compared to the $^4F_{3/2} \rightarrow {}^4I_{9/2}$ transition. It slightly decreases to 0.459 at 1 wt% and then increases to 0.471 with an increase in Nd_2O_3 concentration. Therefore, it is concluded that the efficiency for the $^4F_{3/2} \rightarrow {}^4I_{9/2}$ transition increased and the efficiency for the $^4F_{3/2} \rightarrow {}^4I_{11/2}$ transition decreased as the difference of $\Omega_4 \geq \Omega_6$ is bigger with increase
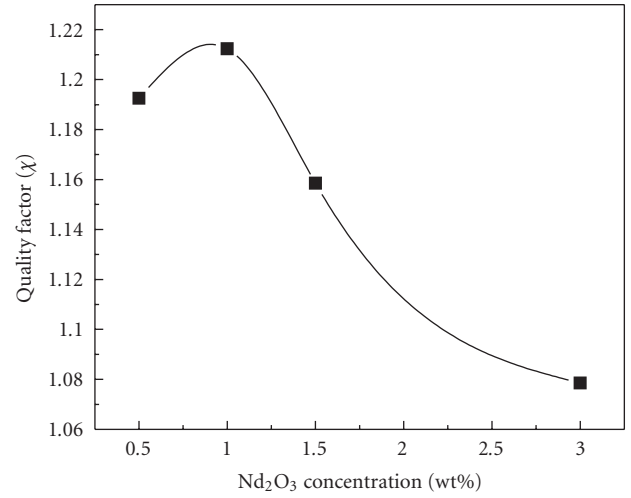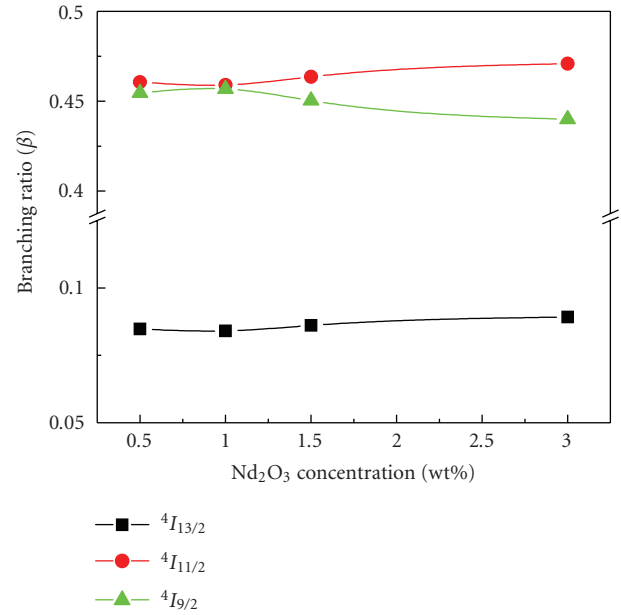
in Nd_2O_3 concentration. Similar values (≈ 0.46) compared to other fluorophosphate glasses have been obtained, which indicated also the potentials for laser host materials for the $^4F_{3/2} \rightarrow {}^4I_{11/2}$ transitions. Figure 7 shows the dependence of $\beta_{J(11/2)}/\beta_{J(13/2)}$ on the spectroscopic quality factor χ for Nd^{3+} ions. The solid line in Figure 7 represents other laser materials. The tendencies of the $\beta_{J(11/2)}/\beta_{J(13/2)}$ are absolutely consistent with that of quality factor shown in Figure 6.
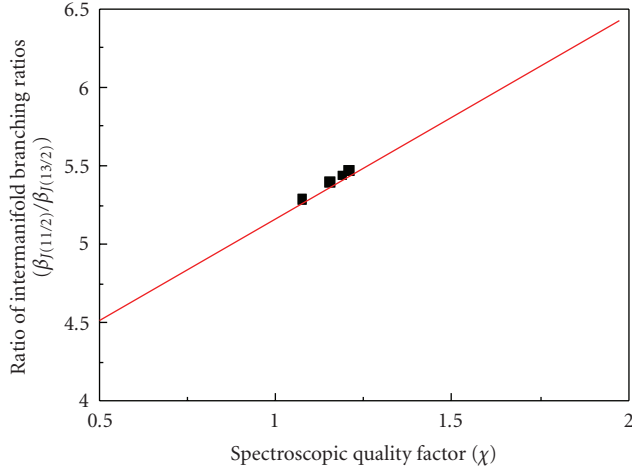
FIGURE 7: Dependence of $\beta_{J(11/2)}/\beta_{J(13/2)}$ on the spectroscopic quality factor χ for Nd^{3+} ions in the Bi(PO$_3$)$_3$−Ba(PO$_3$)$_2$−BaF$_2$−MgF$_2$ glass system.

4.3. Radiative lifetime and stimulated emission cross-section

The radiative lifetimes (τ_{rad}) are related to the total radiative transition probabilities A_{rad} of all transitions from the initial J manifold to the final J' manifold because the transitions from the individual excited state to the lowerlying manifolds should have the same measured lifetime because they all originate from the same excited state. It, therefore, involves the effective average over site-to-site variation of Nd^{3+} ion environment in host materials. Because of the negligible contribution of transition from $^4I_{15/2}$ of Nd^{3+}, the total radiative transition probabilities A_{rad} for three transitions are summed up to obtain the radiative lifetime τ_{rad} from the $^4F_{3/2}$ metastable state using

$$\tau_{\text{rad}}(J) = \frac{1}{\sum_{J'} A(aJ, bJ')}. \tag{9}$$

The values of the radiative lifetime at 1.5 wt% Nd$_2$O$_3$-doped sample are added to obtain the total radiative rates of 188, 1087, and 1189 for the $^4I_{13/2}$, $^4I_{11/2}$, and $^4I_{9/2}$ states, respectively. Therefore, according to (5) the radiative lifetimes of these levels are determined to be 5.31, 92.0, and 84.1 milliseconds, respectively. Radiative lifetimes according to different concentration of Nd$_2$O$_3$ are given in Table 3. Figure 8 shows the variation of stimulated emission cross-section as a function of Nd$_2$O$_3$ concentration. The stimulated cross-section for the $^4F_{3/2} \rightarrow {}^4I_{11/2}$ transition decreases from 3.51×10^{-20} to 1.7×10^{-20} and that for the $^4F_{3/2} \rightarrow {}^4I_{13/2}$ transition also decreases from 6.1×10^{-21} to 3.0×10^{-21}.

4.4. Fluorescence decay rate and quantum efficiency

The relaxation from excited state is represented by both radiative and nonradiative modes. The total transition probability, for example, the reciprocal of the fluorescence decay
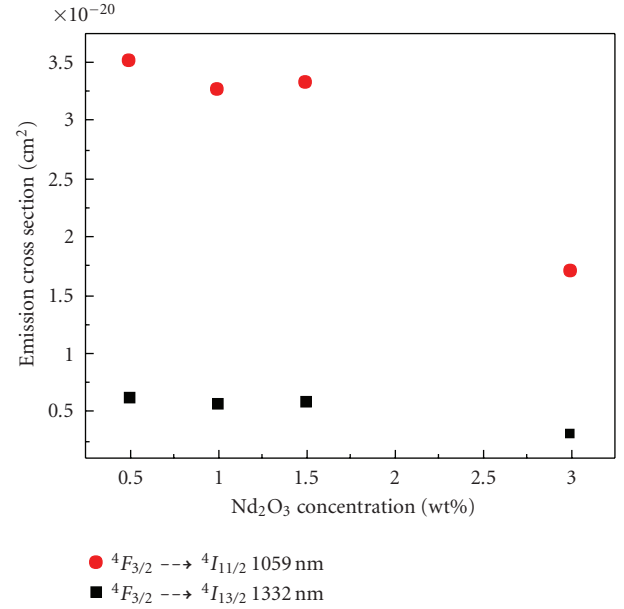

● $^4F_{3/2} \dashrightarrow {}^4I_{11/2}$ 1059 nm
■ $^4F_{3/2} \dashrightarrow {}^4I_{13/2}$ 1332 nm

FIGURE 8: Variation of emission cross section (σ_{em}) as a function of Nd$_2$O$_3$ concentration in the Bi(PO$_3$)$_3$−Ba(PO$_3$)$_2$−BaF$_2$−MgF$_2$ glass system.

lifetime measured ($W_{\text{M}} = 1/\tau$) has the relations with the radiative and nonradiative lifetimes as follows:

$$W_{\text{M}} = W_{\text{R}} + W_{\text{NR}} + W_{\text{E}}. \tag{10}$$

W_{M} is the fluorescence decay rate determined by measuring the lifetime of the $^4F_{3/2} \rightarrow {}^4I_{11/2}$ transition. In the experiments, τ_{med} ($= 1/W_{\text{M}}$) was measured as a function of the Nd^{3+} ion concentration shown in Figure 3. W_{NR} is the nonradiative decay rate due to multiphonon loss and W_{E} are an additional nonradiative decay rate due to the energy transfer processes between Nd^{3+}. As shown in Figure 3, the fluorescence decay curves of the $^4F_{3/2} \rightarrow {}^4I_{11/2}$ transition at 0.5 wt% concentration shows a nonexponential behavior. But the fluorescence decay curves shows exponentially decay at high concentration. The lifetimes were determined by fitting the tail of the decay curve to a single exponential. For direct excitation, radiative quantum efficiency ($\eta = \tau_{\text{med}}/\tau_{\text{rad}}$) of the $^4F_{3/2} \rightarrow {}^4I_{11/2}$ transition is defined as the ratio between emitted light intensity and absorbed pump intensity. Note that radiative quantum efficiency monotonically decrease as a function of Nd$_2$O$_3$ concentration listed in Table 3.

4.5. Multiphonon relaxation analysis

First of all, the nonradiative relaxation of excited states of rare earth ions is through the emission of phonons, where we assume that nonradiative effects due to multiphonon relaxation are negligible at low concentration of Nd^{3+} ions. The nonradiative rate contributed from multiphonon relaxation is given as follows:

$$W_{\text{mp}} = C(1 + n(T))^p \exp(-\alpha \cdot \Delta E), \tag{11}$$

where C is a host dependent constant and p accounts for the effective number of phonons involved in the nonradiative process. ΔE is the energy gap between the $^4F_{3/2}$ and $^4I_{15/2}$ levels. α is represented by a function of $\hbar\omega_{max}$ and the electron-phonon coupling constant as follows:

$$\alpha = -\frac{\ln(\varepsilon)}{\hbar\omega_{max}}, \tag{12}$$

where ε is the ratio of the multiphonon relaxation rate for a p-phonon process W_p to that for $(p-1)$ phonon process W_{p-1} [28]. Since the rate of multiphonon relaxation at a temperature T is influenced by the population of the phonon mode, $n(T) = [\exp(\hbar\omega/kT) - 1]^{-1}$, it is described by Bose-Einstein relation

$$W_{mp}(T) = W_0\left[\frac{\exp(\hbar\omega/kT)}{\exp(\hbar\omega/kT) - 1}\right]^p, \tag{13}$$

where W_0 is obtained at $T = 0$ K and (9). It can be reduced as follows:

$$W_{mp} = W_0\exp(-\alpha\Delta E). \tag{14}$$

In this experiment, W_0 was obtained using the measured lifetimes at 20 K.

In order to calculate the quantitative contribution from multiphonon relaxation to the nonradiative relaxation, IR transmittance spectra were analyzed. The phonon energy, $\hbar\omega$, estimated from strong side band is found to be about 1126 cm^{-1} in this system. The energy gap, ΔE, between $^4F_{3/2}$ and $^4I_{15/2}$ levels is found to be about 5656 cm^{-1}. The number of phonon mode and the value of ε are found to be 5.02 and 0.008, respectively. α calculated using (10) is found to be 4.28×10^{-3} cm. Using above parameters, the multiphonon relaxation rate, W_{mp}, was calculated to be about 73 s^{-1}. Therefore, the multiphonon relaxation until 1 wt% Nd$_2$O$_3$ doped system is reasonably described with a so-called energy gap law assuming the energy transfer is not predominant.

4.6. Energy transfer analysis using Dexter model

On the other hand, the possible explanation for the decrease of fluorescence lifetime of the $^4F_{3/2} \rightarrow {}^4I_{11/2}$ transition can be explained by the energy transfer among Nd^{3+} ions when this concentration increases. Energy transfer from Nd^{3+} ion to another Nd^{3+} ion may result from exchange interaction, radiation reabsorption, or multipole-multipole interaction. Thus, W_E, for example, the additional nonradiative decay rate must be considered. Nonradiative decay rate increases with an increase in Nd^{3+} concentration and the non-radiative decay rate presents a quadratic dependence on Nd^{3+} concentration in current systems as shown in Figure 9, this feature can be analyzed by using the Dexter model which attributes the dominant energy transfer mechanism to the dipole-dipole interactions and proportional to the inverse of the sixth power of the distance separating the two ions and consequently to the squared concentration. According to the selection rules $\Delta J = 0, \pm 1$, only the dipole-dipole interactions are allowed.
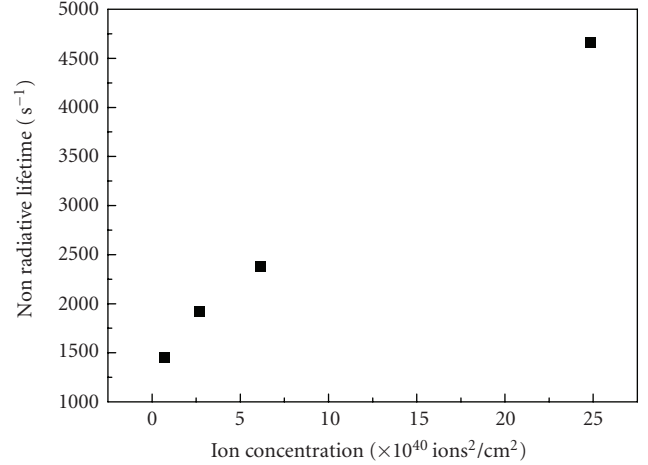

FIGURE 9: Quadratic relation between Nd$_2$O$_3$ concentration and the non-radiative decay rate.

The theoretical expression for the dipole-dipole interactions is as follows:

$$\Phi(t) = \Phi(0)\exp\left[-\frac{t}{\tau} - \frac{4}{3}\pi\Gamma(1/2)N_aR_0^3\left(\frac{t}{\tau}\right)^{3/s}\right], \tag{15}$$

where N is the acceptor concentration, Γ is the Euler function, s is a number which equals 6, and R_0 is a critical radius corresponding to the equality between the nonradiative intrinsic Nd^{3+} relaxation and the transfer rates. The values of τ and R_0 obtained from this simulation are, respectively, almost equal to 178 μs and 8.4 Å. The latter parameter is larger than the mean distance ($R = 7.3$ Å) between Nd^{3+} ions ($R = (3/4\pi N)^{1/3}$) which means that energy transfer is very possible for concentration higher than 4.3×10^{20} cm^{-3}.

5. CONCLUSION REMARKS

The systematic spectroscopic analysis of Nd^{3+} in Bi(PO$_3$)$_3-$Ba(PO$_3$)$_2-$BaF$_2-$MgF$_2$ systems has been performed using Judd-Ofelt theory. It has been found that the intensity parameter Ω_2 for Nd^{3+} slightly decreases from 2.54×10^{-20} to 1.12×10^{-20} (pm^2) with increase in Nd$_2$O$_3$ concentration. The intensity parameters Ω_4, and Ω_6 for Nd^{3+} have been found to decrease from 6.86×10^{-20} to 3.09×10^{-20} and 5.74×10^{-20} to 2.87×10^{-20} (pm^2), respectively, with increasing in Nd$_2$O$_3$ concentration from 0.5 wt% to 3 wt%. It has been found that the efficiency for the $^4F_{3/2} \rightarrow {}^4I_{9/2}$ transition enhances and the efficiency for the $^4F_{3/2} \rightarrow {}^4I_{11/2}$ transition diminishes as the difference between Ω_4 and Ω_6 increases with increasing Nd$_2$O$_3$ concentration. In addition, it has been observed that the emission cross-section for the $^4F_{3/2} \rightarrow {}^4I_{13/2}$ transition decrease from 6.1×10^{-21} to 3.0×10^{-21} (cm^2) and those for the $^4F_{3/2} \rightarrow {}^4I_{11/2}$ transition decreases from 3.51×10^{-20} to 1.7×10^{-20}. The branching ratio for the $^4F_{3/2} \rightarrow {}^4I_{11/2}$ transition will show the opposite trends compared to the $^4F_{3/2} \rightarrow {}^4I_{9/2}$ transition. It slightly decreases to 0.459 at 1 wt% and then increases to 0.471 with increase in Nd$_2$O$_3$ concentration. Therefore, it is concluded that the

efficiency for the $^4F_{3/2} \rightarrow {}^4I_{9/2}$ transition increased and the efficiency for the $^4F_{3/2} \rightarrow {}^4I_{11/2}$ transition decrease as the difference of $\Omega_4 \geq \Omega_6$ is bigger with increase in Nd_2O_3 concentration. Energy transfer from Nd^{3+} ion to another Nd^{3+} ion starts at more than 1 wt% Nd_2O_3 which may result from exchange interaction, radiation reabsorption, or multipole-multipole interaction.

REFERENCES

[1] E. Pecoraro, J. A. Sampaio, L. A. O. Nunes, S. Gama, and M. L. Baesso, "Spectroscopic properties of water free Nd_2O_3-doped low silica calcium aluminosilicate glasses," *Journal of Non-Crystalline Solids*, vol. 277, no. 2-3, pp. 73–81, 2000.

[2] M. Naftaly and A. Jha, "Nd^{3+} -doped fluoroaluminate glasses for a 1.3 μm amplifier," *Journal of Applied Physics*, vol. 87, no. 5, pp. 2098–2104, 2000.

[3] E. Snitzer, "Optical maser action of Nd^{+3} in a barium crown glass," *Physical Review Letters*, vol. 7, no. 12, pp. 444–446, 1961.

[4] S. V. J. Lkshmn and Y. C. Rantnkaran, "Electronic-spectra of the triply ionized neodymium ion in certain sulfate glasses," *Physics and Chemistry of Glasses*, vol. 29, p. 26, 1988.

[5] B. Viana, M. Palazzi, and O. LeFol, "Optical characterization of Nd^{3+} doped sulphide glasses," *Journal of Non-Crystalline Solids*, vol. 215, no. 1, pp. 96–102, 1997.

[6] S. Jiang, T. Luo, B. C. Hwang, et al., "Er^{3+}-doped phosphate glasses for fiber amplifiers with high gain per unit length," *Journal of Non-Crystalline Solids*, vol. 263-264, pp. 364–368, 2000.

[7] D. Ehrt, "Structure and properties of fluoride phosphate glasses," in *Damage to Space Optics, and Properties and Characteristics of Optical Glass*, vol. 1761 of *Proceedings of SPIE*, pp. 213–222, San Diego, Calif, USA, July 1992.

[8] D. Kopf, F. X. Kärtner, U. Keller, and K. J. Weingarten, "Diode-pumped mode-locked Nd: glass lasers with an antiresonant Fabry-Perot saturable absorber," *Optics Letters*, vol. 20, no. 10, pp. 1169–1171, 1995.

[9] W. Vogel, *Glass Chemistry*, chapter 7, Springer, Berlin, Germany, 1992.

[10] A. A. Margaryan, *Ligands and Modifiers in Vitreous Materials*, World Scientific, Singapore, 1999.

[11] A. Margaryan, A. Margaryan, J. H. Choi, and F. G. Shi, "Spectroscopic properties of Mn^{2+} in new bismuth and lead contained fluorophosphate glasses," *Applied Physics B: Lasers and Optics*, vol. 78, no. 3-4, pp. 409–413, 2004.

[12] J. H. Choi, A. Margaryan, A. Margaryan, and F. G. Shi, "Spectroscopic properties of Yb^{3+} in heavy metal contained fluorophosphate glasses," *Materials Research Bulletin*, vol. 40, no. 12, pp. 2189–2197, 2005.

[13] J. H. Choi, A. Margaryan, A. Margaryan, and F. G. Shi, "Judd-Ofelt analysis of spectroscopic properties of Nd^{3+}-doped novel fluorophosphate glass," *Journal of Luminescence*, vol. 114, no. 3-4, pp. 167–177, 2005.

[14] J. H. Choi, A. Margaryan, A. Margaryan, and F. G. Shi, "Optical transition properties of Yb^{3+} in new fluorophosphate glasses with high gain coefficient," *Journal of Alloys and Compounds*, vol. 396, no. 1-2, pp. 79–85, 2005.

[15] J. H. Choi, F. G. Shi, A. Margaryan, and A. Margaryan, "Refractive index and low dispersion properties of new fluorophosphate glasses highly doped with rare-earth ions," *Journal of Materials Research*, vol. 20, no. 1, pp. 264–270, 2005.

[16] B. R. Judd, "Optical absorption intensities of rare-earth ions," *Physical Review*, vol. 127, no. 3, pp. 750–761, 1962.

[17] G. S. Ofelt, "Intensities of crystal spectra of rare-earth ions," *Journal of Chemical Physics*, vol. 37, no. 3, pp. 511–520, 1962.

[18] W. T. Carnall, J. P. Hessler, and F. W. Wagner, "Transition probabilities in the absorption and fluorescence spectra of lanthanides in molten lithium nitrate -potassium nitrate eutectic," *Journal of Physical Chemistry*, vol. 82, no. 20, pp. 2152–2158, 1978.

[19] M. J. F. Digonnet, *Rare Earth Doped Fiber and Amplifiers*, Marcel Dekker, New York, NY, USA, 1993.

[20] G. A. Kumar, A. Martinez, and E. De La Rosa, "Stimulated emission and radiative properties of Nd^{3+} ions in barium fluorophosphate glass containing sulphate," *Journal of Luminescence*, vol. 99, no. 2, pp. 141–148, 2002.

[21] R. C. Powell, *Physics of Solid-State Laser Materials*, Springer, New York, NY, USA, 1998.

[22] H. Ebendorff-Heidepriem, D. Ehrt, M. Bettinelli, and A. Speghini, "Effect of glass composition on Judd-Ofelt parameters and radiative decay rates of Er^{3+} in fluoride phosphate and phosphate glasses," *Journal of Non-Crystalline Solids*, vol. 240, no. 1–3, pp. 66–78, 1998.

[23] C. K. Jørgensen and R. Reisfeld, "Judd-Ofelt parameters and chemical bonding," *Journal of the Less Common Metals*, vol. 93, no. 1, pp. 107–112, 1983.

[24] R. D. Peacock, "The intensities of lanthanide $f \rightarrow f$ transitions," *Structure and Bonding*, vol. 22, pp. 83–122, 1975.

[25] R. R. Jacobs and M. J. Weber, "Dependence of the $^4F_{3/2} \rightarrow {}^4I_{11/2}$ induced-emission cross section for Nd^{3+} on glass composition," *IEEE Journal of Quantum Electronics*, vol. 12, no. 2, part 1, pp. 102–111, 1976.

[26] M. Ajroud, M. Haouari, H. Ben Ouada, H. Maaref, A. Brenier, and C. Garapon, "Investigation of the spectroscopic properties of Nd^{3+}-doped phosphate glasses," *Journal of Physics: Condensed Matter*, vol. 12, no. 13, pp. 3181–3193, 2000.

[27] E. De La Rosa, G. A. Kumar, L. A. Diaz-Torres, A. Martínez, and O. Barbosa-García, "Spectroscopic characterization of Nd^{3+} ions in barium fluoroborophosphate glasses," *Optical Materials*, vol. 18, no. 3, pp. 321–329, 2001.

[28] C. B. Layne, W. H. Lowdermilk, and M. J. Weber, "Multiphonon relaxation of rare-earth ions in oxide glasses," *Physical Review B*, vol. 16, no. 1, pp. 10–20, 1977.

Journal of
Engineering

The Scientific
World Journal

International Journal of
Rotating
Machinery

Journal of
Sensors

International Journal of
Distributed
Sensor Networks

Advances in
Civil Engineering

Journal of
Control Science
and Engineering

Journal of
Robotics

Journal of
Electrical and Computer
Engineering

Advances in
OptoElectronics

VLSI Design

International Journal of
Navigation and
Observation

Modelling &
Simulation
in Engineering

International Journal of
Aerospace
Engineering

International Journal of
Chemical Engineering

International Journal of
Antennas and
Propagation

Active and Passive
Electronic Components

Shock and Vibration

Advances in
Acoustics and Vibration

Hindawi

Submit your manuscripts at
http://www.hindawi.com